RSC Advances

PAPER

View Article Online
View Journal | View Issue

Cite this: *RSC Adv.*, 2021, **11**, 8430

Research on the photoluminescence properties of Cu^{2+}-doped perovskite $CsPbCl_3$ quantum dots†

Ronghua Wu,[a] Zhongchen Bai,[ab] Jinguo Jiang,[a] Heng Yao[a] and Shuijie Qin*[a]

Received 23rd October 2020
Accepted 12th January 2021

DOI: 10.1039/d0ra09043c

rsc.li/rsc-advances

$CsPbX_3$ (X = Cl, Br, and I) quantum dots (QDs) and Cu^{2+}-doped $CsPbCl_3$ QDs with different Cu-to-Pb molar ratios were synthesized *via* a solvent-based thermal synthesis method. The photoluminescence (PL) properties of these Cu^{2+}-doped $CsPbCl_3$ QDs were also investigated in this study. The results showed that with the increase in the Cl^- concentration the surface defects of $CsPb(Cl/Br)_3$ QDs increased, which resulted in an increase in the non-radiative recombination of excitons and weakened the PL intensity. Moreover, Cu^{2+}-doped $CsPbCl_3$ QDs maintained the cubic crystal structure of the initial phases. Owing to the doping of Cu^{2+} ions, the surface defects of $CsPbCl_3$ QDs were effectively eliminated, which facilitated the excitonic recombination *via* a radiative pathway. The PL quantum yields (PLQYs) of Cu^{2+}-doped $CsPbCl_3$ QDs were increased to 51%, showing great photostability. From the results, it is believed that Cu:$CsPbCl_3$ QDs can be widely used in optoelectronic devices.

1 Introduction

All-inorganic cesium lead halide ($CsPbX_3$, X = Cl, Br, and I) quantum dots (QDs) have outstanding physical and chemical properties, such as an adjustable photoluminescence in the visible light range (400–700 nm), narrow emission line width, high fluorescence quantum yields, tolerant point defects and good grain boundaries.[1–7] These characteristics endow the perovskite quantum dots (PQDs) with a promising potential for the applications in optoelectronic devices such as photovoltaics,[8–15] light-emitting diodes (LEDs)[16–21] and lasers.[22–27] Hence, PQDs have aroused widespread research interest. The luminescence color of PQDs can be controlled by either composition or size modulation, and the halogen anion exchange has proven to be an effective strategy to tune the band gap of PQDs instead of destroying the size and crystal structure of its parent nanocrystals.[28]

In addition, the host lattice of $CsPbX_3$ QDs is doped with the transition metal elements to replace a part of the Pb^{2+} ions, which can improve the optical performance.[29–31] However, the practical applications of PQDs in some optoelectronic devices is restricted due to the presence of surface defects, poor stability, and easy oxidation. The elements of Cu and Mn are two representative transition metal elements doped in nanocrystals to improve their optical performance. Mn-doped QDs have stable and high PLQYs (above 50%).[32,33] Since the emission of doped QDs is considered to be derived from the $^4T_1$–$^6A_1$ transition of Mn^{2+}, the emission wavelength is between 580 nm and 600 nm, and the respective luminous color is orange-yellow, which confines their applications. However, compared with Mn-doping, the emission wavelength of the Cu element can be tuned in the visible–near infrared region according to the composition of the main quantum dots.

Srivastava *et al.*[34] prepared Cu:ZnS/$Zn_{1-x}Cd_xS$ QDs with PLQYs of 38%. The PLQYs of Cu:ZnInS/ZnS QDs prepared by Yuan *et al.*[35] exceeded 40%. The PLQYs of Cu-doped CdS QDs prepared by Stouwdam *et al.*[36] exceeded 50%. The Cu:SnO_2 QDs prepared by Babu *et al.*[37] showed a strong absorption in the visible light region. Bi *et al.*[38] prepared $CsPb_{1-x}Cu_xX_3$ QDs (X = Br and Br/Cl) by doping Cu ions into $CsPbX_3$ QDs, which improved their optical characteristics and thermal stability. These results illustrate that Cu^{2+} ions doped into QDs can effectively improve the fluorescence emission efficiency. Herein, we prepared Cu:$CsPbCl_3$ QDs by doping Cu^{2+} into $CsPbCl_3$ QDs, which eliminated the surface defects. We explained the enhancement mechanism of PLQYs from excitonic recombination *via* new radiative pathways. The PLQYs of Cu:$CsPbCl_3$ QDs increased to 51%, exhibiting excellent photostability.

In this study, the synthesis strategy of Cu:$CsPbCl_3$ QDs is depicted in Fig. 1. The rationale is that the metals of $CsCO_3$, $PbCl_2$ and $CuCl_2$ were used as raw materials, which were mixed mechanically at high temperatures. Then, Cu replaced a part of Pb for the synthesis of nanocrystals *via* a solvent-based, thermal synthesis method.

2 Experimental section

2.1 Materials and chemicals

Cs_2CO_3 (Macklin, 99%), $PbCl_2$ (Aladdin, 98%), $PbBr_2$ (Macklin, 99%), PbI_2 (Aladdin, 99%), 1-octadecene (ODE, Aladdin, 90%),

[a]Guizhou Province Key Lab. for Photoelectric Technology and Application, Guizhou University, Guiyang City, 550025, People's Republic of China

[b]College of Medicine, Guizhou University, Guiyang City, 550025, People's Republic of China

† Electronic supplementary information (ESI) available. See DOI: 10.1039/d0ra09043c

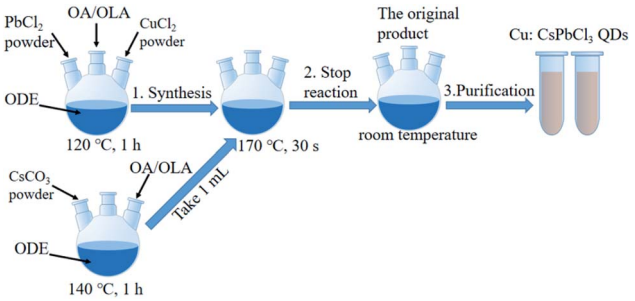

Fig. 1 Schematic of the synthesis of Cu:$CsPbCl_3$ QDs.

oleic acid (OA, Aladdin, 90%), oleylamine (OLA, Aladdin, 80–90%), $CuCl_2$ (Jinshan, 99%), and *n*-hexane (Fuyu, 98%) were purchased. All chemicals were used without any further purification.

2.2 Preparation of the Cs-oleate solution

2.5 mL OA, 30 mL ODE and Cs_2CO_3 (0.8 g, 2.5 mmol) powder were put into a 100 mL three-neck flask at 140 °C for 1 h under magnetic stirring until the Cs_2CO_3 powder completely dissolved and the solution became transparent.

2.3 Synthesis of $CsPbX_3$ QDs

1.5 mL OA, 1.5 mL OLA and 15 mL ODE, and 0.15 g, 0.54 mmol $PbCl_2$, 0.2 g, 0.54 mmol $PbBr_2$, 0.25 g, 0.54 mmol PbI_2, $PbCl_2$/$PbBr_2$ with specific molar ratios were loaded into a 100 mL three-necked flask and heated at 120 °C for 1 h to obtain $CsPbCl_3$ QDs, $CsPbBr_3$ QDs, $CsPbI_3$ QDs, $CsPb(Cl/Br)_3$ QDs, respectively. After the reaction temperature was increased to 170 °C, the Cs-oleate solution (1 mL) was quickly injected for reacting and after 30 s, the solution was cooled to room temperature in an ice bath.

2.4 Synthesis of Cu:$CsPbCl_3$ QDs

We prepared Cu:$CsPbCl_3$ QDs with the molar ratios of $CuCl_2$ and $PbCl_2$ of 0.1 : 1, 0.3 : 1, 0.5 : 1, 0.9 : 1, and 1.7 : 1. The typical synthetic procedure of Cu:$CsPbCl_3$ QDs with the Cu-to-Pb molar ratio of 0.9 : 1 as follows: 1.5 mL OA, 1.5 mL OLA, 15 mL ODE, $PbCl_2$ (0.097 g, 0.35 mmol) and $CuCl_2$ (0.053 g, 0.31 mmol) powders were loaded in a 100 mL three-neck flask heated to 120 °C for 1 h. The reaction temperature was increased to 170 °C, and the Cs-oleate solution (1 mL) was quickly injected, and after 30 s, the reaction was cooled to room temperature on an ice bath.

2.5 Purification

$CsPbX_3$ and Cu:$CsPbCl_3$ QDs were extracted from the original product *via* centrifugation at 8000 rpm for 5 min, and the precipitate was taken out. The resulting precipitates were dispersed in *n*-hexane at room temperature and were centrifuged for 5 min at a speed of 6000 rpm; the supernatant was taken, and this process was repeated twice to get $CsPbX_3$ and Cu:$CsPbCl_3$ QDs. Then, they were kept aside for 24 h in a freezer, and were taken out again for centrifugal purification, obtaining a clear colloidal $CsPbX_3$ and Cu:$CsPbCl_3$ QDs.

2.6 Characterization and spectral analysis

PL spectra were obtained on a Cary Eclipse-G9800A Fluorescence Spectrophotometer from Agilent Technologies. UV-Visible (UV-Vis) spectroscopy was performed using a UV-2700 UV-Vis Spectrophotometer from Shimadzu. The doping concentrations of Cu^{2+} were monitored by an Agilent inductively coupled plasma-optical emission spectrometer 730 (ICP-OES730). Dried powdered samples of QDs were acid-digested and then diluted prior to measurements. The crystal structures were characterized on a Jeol-2100f transmission electron microscope (TEM) at 200 kV. TEM specimens were prepared by directly drying a drop of a dilute *n*-hexane solution of PQDs on the surface of a carbon-coated copper grid. Energy dispersive X-ray (EDX) measurements were performed using X-max 80 from Oxford Instruments. X-ray photoelectron spectroscopy (XPS) characterizations were conducted on a Thermo Scientific ESCALAB 250Xi spectrometer using a monochromatic Al Kα radiation source (200 W), where the sample were prepared directly by drying a drop of dilute *n*-hexane solution of PQDs onto an Si wafer. X-ray diffraction (XRD) measurements were performed by a Rigaku SmartLab XG X-ray diffractometer. XRD specimens were prepared by directly drying a drop of the dilute *n*-hexane solution of PQDs onto a glass slide. The room temperature PLQYs of PQDs were calculated by comparing the integrated emission of the PQD samples in an *n*-hexane solution with that of rhodamine 6G with the PLQYs of 95% in ethanol with identical optical density. Fourier transform infrared (FTIR) spectrum was obtained using a VERTEX70 Spectrometer from Bruker.

3 Results and discussions

3.1 The PL and UV-Vis absorption spectra of $CsPbX_3$ QDs

The PL and UV-Vis absorption spectra of $CsPbX_3$ QDs are shown in Fig. 2a and b. The PL intensity of $CsPbCl_3$ QDs was much lower than that of $CsPbBr_3$ and $CsPbI_3$ QDs. Owing to the surface of perovskite $CsPbCl_3$, QDs have a serious local trap states,[39] which produced non-radiative recombination and resulted in a weak PL intensity. The peaks of excitonic absorption from $CsPbCl_3$, $CsPbBr_3$ and $CsPbI_3$ QDs were located at 395 nm, 469 nm and 676 nm, respectively. The red shift in the absorption peaks was caused by the weak binding ability of the halogen element.

In order to observe the PL spectra of PQDs mixed with halogen elements, we prepared a series of $CsPb(Cl/Br)_3$ QDs mixed with different Cl-to-Br molar ratios. The PL spectra and UV-Vis absorption spectra of these QDs are shown in Fig. 2c and d, respectively. The PL intensity of $CsPb(Cl/Br)_3$ QDs decreased gradually with the increase in the Cl^- ion concentrations, and the peaks of exciton emission were blue-shifted. There were Pb–Cl ion vacancies on the surface of $CsPbCl_3$ QDs, which seriously reduced its PL efficiency.[32] This illustrated that as the concentration of Cl^- ions increased, the number of Pb–Cl ion vacancies on the surface also increased. This led to the non-radiative recombination of QD excitons and reduced the PL intensity of $CsPb(Cl/Br)_3$ QDs. The peak of excitonic absorption was also blue-shifted with the increase in Cl^- ion concentrations. The divalent Cu^{2+} in the transition metal series has a smaller ionic

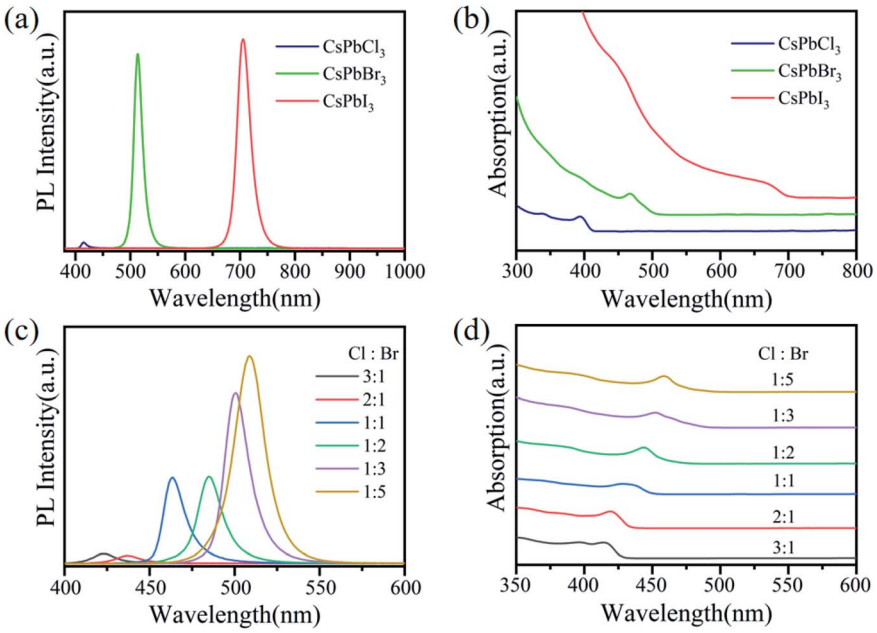

Fig. 2 (a) The PL spectra of $CsPbX_3$ QDs. (b) Absorption spectra of $CsPbX_3$ QDs. (c) The PL spectra of $CsPb(Cl/Br)_3$ QDs with different Cl-to-Br molar ratios. (d) UV-Vis absorption spectra of $CsPb(Cl/Br)_3$ QDs with different Cl-to-Br molar ratios.

radius (73 pm) and can be used as a good doping element to eliminate the surface defects of the quantum dots.

To eliminate the surface defects of $CsPbCl_3$ QDs for improving its fluorescence emission efficiency and photostability, we further doped the divalent metal Cu^{2+} ion in the $CsPbCl_3$ QDs to increase the proportion of copper ions.

3.2 TEM images

In order to illustrate the effects of Cu^{2+}-doped on the surface structure of $CsPbCl_3$ QDs, the TEM images of undoped and Cu^{2+}-doped $CsPbCl_3$ QDs are shown in Fig. 3a and b. The structural morphologies of Cu^{2+}-doped $CsPbCl_3$ QDs were of cubic crystal structure as $CsPbCl_3$ QDs. These are in line with the crystal phase of PQDs prepared under the conditions of high temperature synthesis and QD surface effects.[16,40] Fig. 3c and d show their HRTEM images with clear lattice fringes. As measured from their crystal plane spacings of 0.283 nm and 0.280 nm, it was found that they corresponded to (002) lattice plane of $CsPbCl_3$ QDs. These results indicate that Cu^{2+}-doped $CsPbCl_3$ QDs maintain the crystal structure of the initial phases and shrink the surface lattice spacing, improving the crystallinity of QDs.

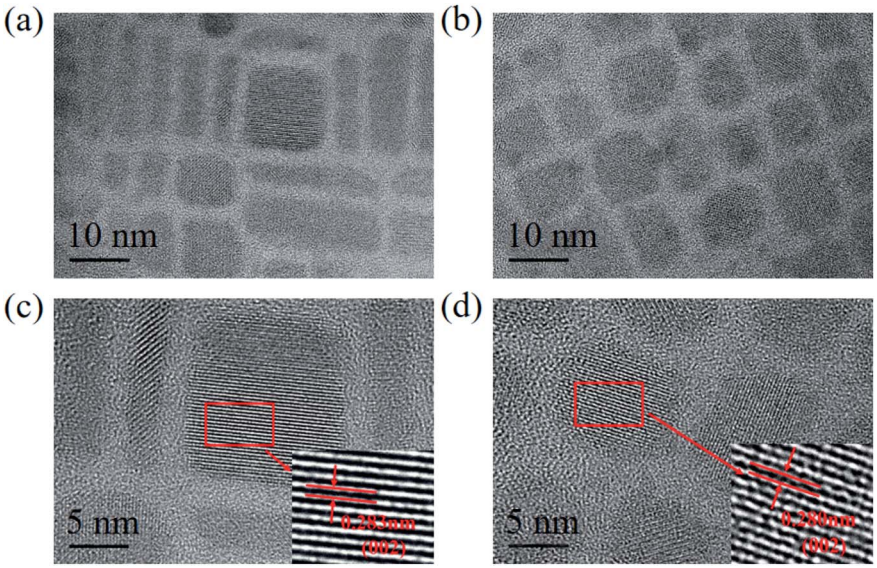

Fig. 3 (a) TEM images of $CsPbCl_3$ QDs. (b) TEM images of Cu^{2+}-doped $CsPbCl_3$ QDs with the Cu-to-Pb molar ratio of 0.9 : 1. (c) HRTEM micrograph of $CsPbCl_3$ QDs. (d) HRTEM micrograph of Cu^{2+}-doped $CsPbCl_3$ QDs with the Cu-to-Pb molar ratio of 0.9 : 1.

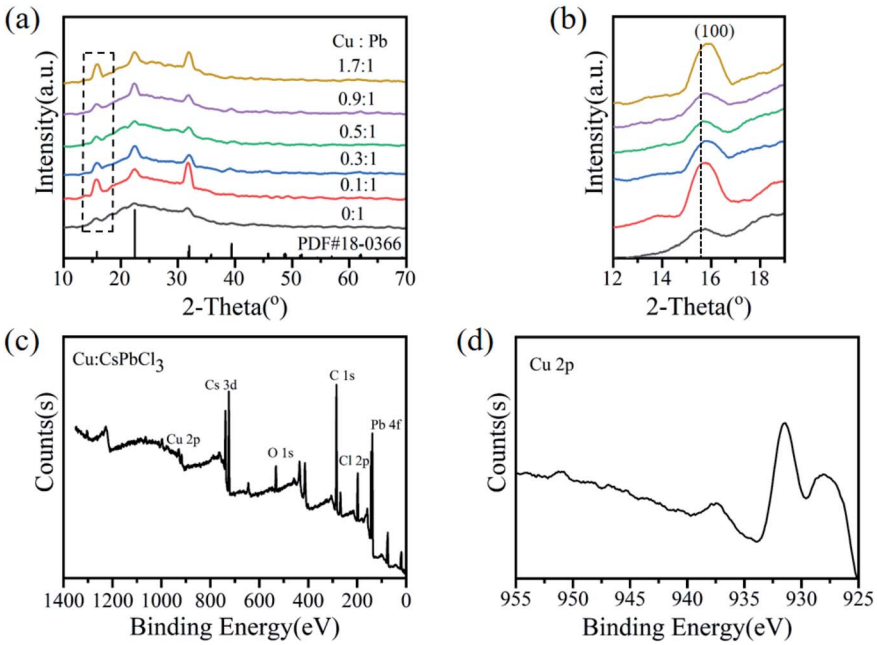

Fig. 4 (a) XRD patterns of Cu^{2+}-doped $CsPbCl_3$ QDs with different Cu-to-Pb molar ratios. (b) Enlarged the XRD patterns of the 2-theta degree. (c) XPS spectrum of Cu:$CsPbCl_3$ with the Cu-to-Pb molar ratio of 0.9 : 1. (d) The high-resolution XPS spectrum of Cu 2p.

3.3 XRD, XPS and EDX spectra

The typical XRD patterns further confirmed that the Cu:$CsPbCl_3$ QDs prepared by different Cu-to-Pb molar ratios retained the same crystalline structure of tetragonal $CsPbCl_3$ QDs, as shown in Fig. 4a. The diffraction characteristic peaks of undoped and Cu^{2+}-doped $CsPbCl_3$ QDs are similar, which correspond to the standard XRD spectra of $CsPbCl_3$ QDs (PDF #18-0366). The peak positions of (100) moved to higher 2-theta degree values (shown in Fig. 4b) with the increase in the Cu^{2+} ion concentrations, which indicate that the lattice contraction and the lattice parameters became smaller.[38] These results show that some of the larger Pb^{2+} (119 pm) ions in $CsPbCl_3$ QDs were replaced by smaller Cu^{2+} (73 pm) ions. The doping concentrations of Cu ions were measured *via* ICP-OES (Table S1†). When Cu^{2+}-doped $CsPbCl_3$ QDs with the Cu-to-Pb molar ratio of 0.9 : 1, its PLQYs reached 51%. Also, the doping concentration of Cu ions relative

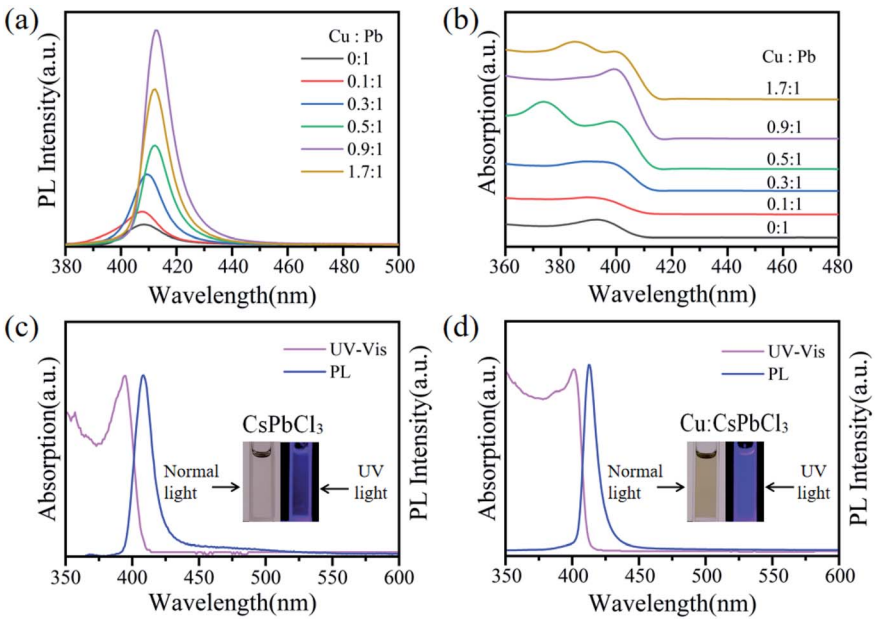

Fig. 5 (a) PL spectra of Cu^{2+}-doped $CsPbCl_3$ QDs with different Cu-to-Pb molar ratios. (b) UV-Vis absorption spectra of Cu^{2+}-doped $CsPbCl_3$ QDs with different Cu-to-Pb molar ratios. (c) UV-Vis absorption and PL spectra of $CsPbCl_3$ QDs. (d) UV-Vis absorption and PL spectra of Cu^{2+}-doped $CsPbCl_3$ QDs with the Cu-to-Pb molar ratio of 0.9 : 1; the insets show photographs under normal light and 365 nm excitation.

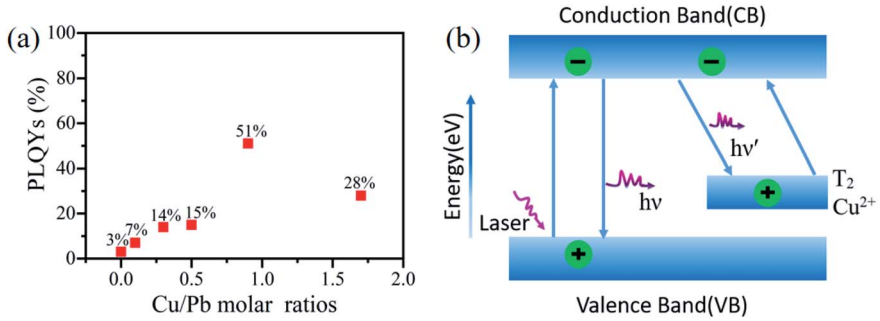

Fig. 6 (a) PLQYs of Cu^{2+}-doped $CsPbCl_3$ QDs with different Cu-to-Pb molar ratios. (b) Schematic showing the pathways of radiative recombination of the introduction of Cu^{2+} states within the host band gap.

to Pb ions was 2.32%. The EDX spectrum of Cu^{2+}-doped $CsPbCl_3$ QDs with the Cu-to-Pb molar ratio of 0.9 : 1 is shown in Fig. S1a,† the presence of Pb, Cs, Cu and Cl elements were observed. The XPS spectrum of Cu:$CsPbCl_3$ QDs with the Cu-to-Pb molar ratio of 0.9 : 1 is shown in Fig. 4c, which exhibited XPS peaks of Cu 2p, Cs 3d, Pb 4f, Cl 2p, C 1s and O 1s. Furthermore, the high-resolution XPS spectra (Fig. 4d) reveal that the binding energy (BE) is 931.5 eV for Cu $2p_{3/2}$, and the BE peak at 937.5 eV is the characteristic Cu^{2+} shake-up satellite peak.[41] In addition, the BE at 738.4 eV and 724.4 eV are for Cs $3d_{3/2}$ and Cs $3d_{5/2}$, 143.1 eV and 138.2 eV for Pb $4f_{5/2}$ and Pb $4f_{7/2}$, 199.4 eV and 197.8 eV for Cl $2p_{1/2}$ and Cl $2p_{3/2}$, respectively, as shown in Fig. S1b–d.† These results suggest that Cu^{2+} was successfully doped into $CsPbCl_3$ QDs.

3.4 The PL and UV-Vis absorption spectra of Cu:$CsPbCl_3$ QDs

Fig. 5a depicts the PL spectra of Cu^{2+}-doped $CsPbCl_3$ QDs with different Cu-to-Pb molar ratios. It is observed that as the Cu^{2+} ion concentration increased, the PL intensity of Cu^{2+}-doped $CsPbCl_3$ QDs also increased and then gradually decreased. Their emission peaks display a redshift from 408 nm to 412 nm. When the Cu-to-Pb molar ratio reached 1.7 : 1, the PL intensity of Cu:$CsPbCl_3$ QDs weakened. This indicates that excessive doping of Cu^{2+} ions form a non-radiative relaxation channel in $CsPbCl_3$ QDs leads to the decrease in the PL intensity. It can be observed from the Urbach tails in the UV-Vis absorption spectra shown in Fig. 5b that the absorption edge of doped Cu^{2+} ions was steeper than that of undoped QDs, which confirmed that the system was disordered or the defects were reduced.[42,43] This is consistent with the enhancement of the PL intensity of excitonic emission. In the case mentioned above, the redshifts of the PL and absorption spectra of Cu^{2+}-doped $CsPbCl_3$ QDs are caused by the recombination of electrons in the conduction band of the host material and holes in the Cu^{2+} T_2 state.[34,44,45] These results confirmed that doping Cu^{2+} with an ionic radius of 73 pm forms Cu–Cl ion pairs to fill the Pb–Cl ion vacancies, effectively eliminating the non-radiative recombination of excitons, which enhanced the PL intensity of $CsPbCl_3$ QDs.

Fig. 5c and d show the UV absorption and PL spectra of undoped and Cu^{2+}-doped $CsPbCl_3$ QDs with the Cu-to-Pb molar ratio of 0.9 : 1, respectively. As shown in the both figures, the full width at half maxima (FWHM) of the PL spectra of Cu^{2+}-doped was narrower (12 nm) than that of the undoped $CsPbCl_3$ QDs (16 nm), which illustrated that the size distribution of the PQD nanoparticles and homogeneity of the morphology were improved. From the photographs of these solutions under 365 nm excitation, the blue-violet light emitted by Cu^{2+}-doped under the excitation of the laser was obviously brighter than the undoped $CsPbCl_3$ QDs. Fig. 6a shows the PLQYs of Cu^{2+}-doped $CsPbCl_3$ QDs with numerous molar ratios of Cu-to-Pb (0 : 1, 0.1 : 1, 0.3 : 1, 0.5 : 1, 0.9 : 1 and 1.7 : 1), increasing from 3% to 51%.

3.5 The mechanism model of enhanced PL

According to the above-mentioned results, the mechanism model of enhanced PL of Cu:$CsPbCl_3$ QDs is shown in Fig. 6b. Under the excitation of 365 nm laser, the $CsPbCl_3$ QD host absorbs energy and emits a 408 nm blue-violet light *via* the radiative recombination of excitons between the valence band (VB) and the conduction band (CB). Due to the presence of defect trap states, the non-radiative recombination pathway of excitons leads to energy loss. Hence, Cu^{2+} is introduced to recombine the excitons with a new radiation pathway. A part of the electrons in the conduction band of the $CsPbCl_3$ host are transferred to the Cu^{2+} T_2 state and recombined with the holes in this energy state, forming a new excitonic recombination pathway.[46,47] It leads to the red-shift in the PL emission peak. Furthermore, the Cu^{2+} T_2 states absorb energy and then pump the electrons to transition to the conduction band of the host. The energy transfer of the photoinduced excitons from the $CsPbCl_3$ QD host to the Cu^{2+} T_2 state, which promotes the

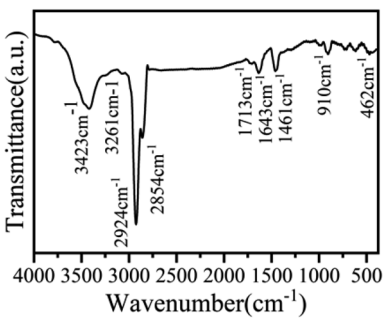

Fig. 7 FTIR spectrum of Cu:$CsPbCl_3$ QDs with Cu-to-Pb molar ratio of 0.9 : 1.

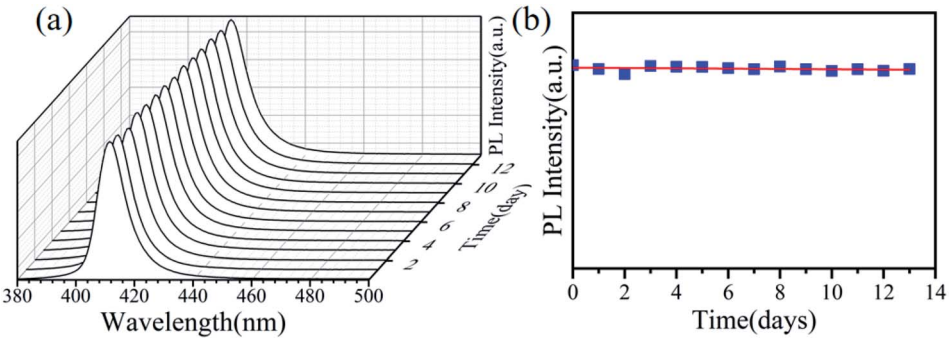

Fig. 8 PL spectra of Cu:$CsPbCl_3$ QDs with the Cu-to-Pb molar ratio of 0.9 : 1 over time (days): (a) the PL spectra and (b) fitting of the PL intensity.

recombination of excitons *via* the radiative pathway, reduces energy loss, and enhances the PL intensity.

3.6 FTIR analysis

Chemical components of Cu:$CsPbCl_3$ QDs were also analyzed. Some chemical elements can be observed in the FTIR spectrum, as shown in Fig. 7. The peaks at 3423 cm^{-1} and 1713 cm^{-1} are the stretching vibration peaks of the O–H and C=O bonds, which confirm that the ligand shell of PQDs contains oleic acid molecules. The peaks at 2924 cm^{-1} and 2854 cm^{-1} and 910 cm^{-1} are the vibration peaks of the olefin C–H bond. A weak stretching vibration peak of the N–H bond was observed at 3261 cm^{-1}, which illustrates that the ligand shell of PQDs contains oleylamine molecules. The peak at 1643 cm^{-1} is the stretching vibration peak of the C=C bond, while the peak at 462 cm^{-1} is the vibration peak of the Pb–O bond, which is due to the carboxyl combines with the Pb^{2+} ions. These results show that Cu:$CsPbCl_3$ QDs are packaged by OA and OLA, which can combine with other materials *via* adsorption or chemical bonds.[48–50] This is significant for the preparation of highly conductive quantum dot films for photovoltaics and LED applications. In addition, the peak at 1461 cm^{-1} is the bending vibrations of the alkane C–H bond, which is because Cu:$CsPbCl_3$ QDs were dispersed in *n*-hexane.

3.7 Photostability

We further explored the photostability of Cu:$CsPbCl_3$ QDs, and the PL spectra of the sample with a Cu-to-Pb molar ratio of 0.9 : 1 were measured for two consecutive weeks. In Fig. 8a, the Cu:$CsPbCl_3$ QD PL emission slightly redshifted by 2 nm with the increase in time (days). Also, the fitting curve of the PL intensity over time is shown in Fig. 8b. It can be seen that the PL intensity increases over time and still remains relatively stable, which proved that the Cu^{2+}-doped $CsPbCl_3$ QDs have a good photostability.

4 Conclusions

In summary, we have successfully synthesized $CsPbX_3$ and Cu^{2+}-doped $CsPbCl_3$ QDs *via* a the solvent-based thermal synthesis method. The results clearly show that the PL intensity of blue-violet light-emitting $CsPbX_3$ QDs was much lower than that of green and red light-emitting. With the increase in the concentration of Cl^- ions, the number of surface defects of $CsPb(Cl/Br)_3$ QDs increased, which facilitated the non-radiative recombination of excitons and weakened the PL intensity of QDs. Cu^{2+}-doped facilitated the exciton recombination *via* a radiative pathway that effectively enhanced the PLQYs of $CsPbCl_3$ QDs from 3% to 51%, while maintaining the cubic crystal structure surface morphology. Moreover, the full width at half maxima of the PL spectra of Cu^{2+}-doped $CsPbCl_3$ QDs was narrower than that of the undoped $CsPbCl_3$ QDs, which further proved that Cu^{2+}-doped improves the crystallinity of $CsPbCl_3$ QDs and reduces surface defects. We further tested the photostability of Cu:$CsPbCl_3$ QDs. The sample QDs showed relatively stable PL intensity for two consecutive weeks. These results show that Cu:$CsPbCl_3$ QDs can be widely used in the field of optoelectronic devices.

Conflicts of interest

The authors have declared that no conflicting interests exist.

Acknowledgements

This works were supported by National Natural Science Foundation of China (NSFC) (61865002 and 62065002); Project of outstanding young scientific and technological talents of Guizhou Province (QKEPTRC[2019]5650); Guizhou Province Science and Technology Project (QKHZ [2017]2887); Central Government of China Guiding Local Science and Technology Development Plan (QKZYD[2017]4004).

References

1 Y. Wei, X. R. Deng, Z. X. Xie, X. C. Cai, S. S. Liang, P. Ma, Z. Y. Hou, Z. Y. Cheng and J. Lin, *Adv. Funct. Mater.*, 2017, **27**(39), 1703535.
2 J. Pan, S. P. Sarmah, B. Murali, I. Dursun, W. Peng, M. R. Parida, J. Liu, L. Sinatra, N. Alyami, C. Zhao, E. Alarousu, T. K. Ng, B. S. Ooi, O. M. Bakr and O. F. Mohammed, *J. Phys. Chem. Lett.*, 2015, **6**(24), 5027–5033.
3 N. S. Makarov, S. Guo, O. Isaienko, W. Liu, I. Robel and V. I. Klimov, *Nano Lett.*, 2016, **16**, 2349–2362.
4 C. C. Lin, K. Y. Xu, D. Wang and A. Meijerink, *Sci. Rep.*, 2017, **7**(1), 45906.

5 H. Wang, N. Sui, X. Bai, Y. Zhang, Q. Rice, F. J. Seo, Q. B. Zhang, V. L. Colvin and W. W. Yu, *J. Phys. Chem. Lett.*, 2018, **9**(15), 4166–4173.
6 L. Protesescu, S. Yakunin, M. I. Bodnarchuk, F. Krieg, R. Caputo, C. H. Hendon, R. X. Yang, A. Walsh and M. V. Kovalenko, *Nano Lett.*, 2015, **15**(6), 3692–3696.
7 M. Shekhirev, J. Goza, J. D. Teeter, A. Lipatov and A. Sinitskii, *J. Chem. Educ.*, 2017, **94**(8), 1150–1156.
8 S. S. Mali and C. K. Hong, *Nanoscale*, 2016, **8**, 10528–10540.
9 D. L. Zhou, D. L. Liu, G. C. Pan, X. Chen, D. Y. Li, W. Xu, X. Bai and H. W. Song, *Adv. Mater.*, 2017, **29**, 1704149.
10 U. Rau, *Phys. Rev. B: Condens. Matter Mater. Phys.*, 2007, **76**(8), 85303.
11 Y. Li, Z. W. Wang, D. Ren, Y. H. Liu, A. B. Zheng, S. M. Zakeeruddin, X. D. Dong, A. Hagfeldt, M. Gratzel and P. Wang, *ACS Appl. Energy Mater.*, 2019, **2**(5), 3822–3829.
12 W. Ahmad, J. Khan, G. Niu and J. Tang, *Sol. RRL*, 2017, **1**(7), 1700048.
13 E. Bi, H. Chen, F. Xie, Y. Wu, W. Chen, Y. Su, A. Islam, M. GraTzel, X. Yang and L. Han, *Nat. Commun.*, 2017, **8**(1), 15330.
14 J. Wang, J. Zhang, Y. Zhou, H. Liu and A. K. Y. Jen, *Nat. Commun.*, 2020, **11**(1), 177.
15 E. M. Sanehira, A. R. Marshall, J. A. Christians, S. P. Harvey and J. M. Luther, *Sci. Adv.*, 2017, **3**(10), eaao4204.
16 A. Swarnkar, A. R. Marshall, E. M. Sanehira, B. D. Chernomordik and D. T. Moore, *Science*, 2016, **354**(6308), 92–95.
17 J. Z. Song, J. H. Li, X. Ming, L. M. Xu, Y. H. Dong and H. B. Zeng, *Adv. Mater.*, 2015, **27**(44), 7162–7167.
18 X. X. Di, Z. Hu, J. T. Jiang, M. L. He, L. Zhou, W. D. Xiang and X. J. Liang, *Chem. Commun.*, 2017, **53**(80), 11068–11071.
19 T. Matsushima, F. Bencheikh, T. Komino, M. R. Leyden, A. S. D. Sandanayaka, C. Qin and C. Adachi, *Nature*, 2019, **572**, 502–506.
20 K. Sim, T. Jun, J. Bang, H. Kamioka and H. Hosono, *Appl. Phys. Rev.*, 2019, **6**(3), 031402.
21 K. B. Lin, J. Xing, L. N. Quan, *et al.*, *Nature*, 2018, **562**(7726), 245–248.
22 X. J. Huang, Q. Y. Guo, D. D. Yang, X. D. Xiao, G. P. Dong, *et al.*, *Nat. Photonics*, 2020, **14**(2), 82–88.
23 J. Chen, Y. Wu, X. M. Li, F. Cao, Y. Gu, K. Liu, X. H. Liu, Y. H. Dong, J. P. Ji and H. B. Zeng, *Adv. Mater. Technol.*, 2017, **2**(10), 1700132.
24 C. Y. Huang, C. Zou, C. Y. Mao, K. L. Corp, Y. C. Yao, Y. J. Lee, C. W. Schlenker, K. Y. Jen and L. Y. Lin, *ACS Photonics*, 2017, **4**(9), 2281–2289.
25 J. Z. Li, H. X. Dong, B. Xu, S. F. Zhang, Z. P. Cai, J. Wang and L. Zhang, *Photonics Res.*, 2017, **5**(5), 457–460.
26 X. S. Tang, Z. P. Hu, W. W. Chen, X. Xing, L. Q. Mai, *et al.*, *Nano Energy*, 2016, **28**, 462–468.
27 Y. Wang, X. M. Li, J. Z. Song, L. Xiao, H. B. Zeng and H. D. Sun, *Adv. Mater.*, 2015, **27**(44), 7101–7108.
28 G. Nedelcu, L. Protesescu, S. Yakunin, M. I. Bodnarchuk, M. J. Grotevent and M. V. Kovalenko, *Nano Lett.*, 2015, **15**(8), 5635–5640.
29 H. Chung, S. I. Jung, H. J. Kim, W. Cha, E. Sim, D. Kim, W. K. Koh and J. Kim, *Angew. Chem., Int. Ed. Engl.*, 2017, **56**(15), 4160.
30 D. Q. Chen, G. L. Fang and X. Chen, *ACS Appl. Mater. Interfaces*, 2017, **9**(46), 40477–40487.
31 W. J. Mir, Y. Mahor, A. Lohar, M. Jagadeeswararao, S. Das, S. Mahamuni and A. Nag, *Chem. Mater.*, 2018, **30**(20), 8170–8178.
32 H. W. Liu, Z. N. Wu, J. R. Shao, D. Yao, H. Gao, Y. Liu, W. L. Yu, H. Zhang and B. Yang, *ACS Nano*, 2017, **11**(2), 2239–2247.
33 D. Parobek, B. J. Roman, Y. T. Dong, H. Jin, E. Lee, M. Sheldon and D. H. Son, *Nano Lett.*, 2016, **16**(12), 7376–7380.
34 B. B. Srivastava, S. Jana and N. Pradhan, *J. Am. Chem. Soc.*, 2011, **133**(4), 1007–1015.
35 X. Yuan, J. Hua, R. S. Zeng, D. H. Zhu, W. Y. Ji, P. T. Jing, X. D. Meng, J. L. Zhao and H. B. Li, *Nanotechnology*, 2014, **25**(43), 435202.
36 J. W. Stouwdam and R. A. J. Janssen, *Adv. Mater.*, 2009, **21**(28), 2916–2920.
37 B. Babu, A. N. Kadam, R. V. S. S. N. Ravikumar and C. Byon, *J. Alloys Compd.*, 2017, **703**, 330–336.
38 C. H. Bi, S. X. Wang, Q. Li, S. V. Kershaw, J. J. Tian and A. L. Rogach, *J. Phys. Chem. Lett.*, 2019, **10**(5), 943–952.
39 G. H. Ahmed, J. K. El-Demellawi, Y. Jun, P. Jun, V. D. Velusamy, M. N. Hedhili, E. Alarousu, O. M. Bakr, H. N. Alshareef and O. F. Mohammed, *ACS Energy Lett.*, 2018, **3**(10), 2301–2307.
40 Q. A. Akkerman, S. G. Motti, A. R. S. Kandada, E. Mosconi, V. D'Innocenzo, G. Bertoni, S. Marras, B. A. Kamino, L. Miranda, F. De Angelis, A. Petrozza, M. Prato and L. Manna, *J. Am. Chem. Soc.*, 2016, **138**(3), 1010–1016.
41 P. Liu and E. J. M. Hensen, *J. Am. Chem. Soc.*, 2013, **135**(38), 14032–14035.
42 P. Guyot-Sionnest, E. Lhuillier and H. Liu, *J. Chem. Phys.*, 2012, **137**(15), 154704.
43 J. Pal, A. Bhunia, S. Chakraborty, S. Manna, S. Das, A. Diwan, S. Datta and A. Nag, *J. Phys. Chem. C*, 2018, **22**(19), 10643–10649.
44 S. Cao, W. Y. Ji, J. L. Zhao, W. Y. Yang, C. M. Li and J. J. Zheng, *J. Mater. Chem. C*, 2016, **4**(3), 581–588.
45 W. J. Zhang, Q. Lou, W. Y. Ji, J. L. Zhao and X. H. Zhong, *Chem. Mater.*, 2014, **26**(2), 1204–1212.
46 G. K. Grandhi and R. Viswanatha, *J. Phys. Chem. Lett.*, 2013, **4**(3), 409–415.
47 A. M. Jawaid, S. Chattopadhyay, D. J. Wink, L. E. Page and P. T. Snee, *ACS Nano*, 2013, **7**(4), 3190–3197.
48 Z. C. Bai, J. Zhou, M. Peng, Z. P. Zhang and S. J. Qin, *J. Opt. Soc. Am. B*, 2019, **36**(6), 1420–1428.
49 Z. L. Liu, C. Chang, W. J. Zhang, M. Yang and Q. Zhang, *IOP Conf. Ser.: Mater. Sci. Eng.*, 2019, **562**, 012067.
50 B. Fritzinger, R. K. Capek, K. Lambert, J. C. Martins and Z. Hens, *J. Am. Chem. Soc.*, 2010, **132**(29), 10195–10201.